Efficient generation of subnatural-linewidth biphotons by controlled quantum interference

Ravikumar Chinnarasu,* Chi-Yang Liu, Yi-Feng Ding, Chuan-Yi Lee, Tsung-Hua Hsieh, Ite A. Yu, and Chih-Sung Chuu†
Department of Physics, National Tsing Hua University, Hsinchu 30013, Taiwan
and Center for Quantum Technology, Hsinchu 30013, Taiwan

(Received 10 June 2019; accepted 3 June 2020; published 29 June 2020)

Biphotons of narrow bandwidth and long temporal length play a crucial role in long-distance quantum communication (LDQC) and linear optical quantum computing (LOQC). However, generation of these photons usually requires atomic ensembles with high optical depth or spontaneous parametric down-conversion with sophisticated optical cavity. By manipulating the two-component biphoton wave function generated from a low-optical-depth (low-OD) atomic ensemble, we demonstrate biphotons with subnatural linewidth in the sub-MHz regime. The potential to shape and manipulate the quantum wave packets of these temporally long photons is also demonstrated and discussed. Our work has potential applications in realizing quantum repeaters and large cluster states for LDQC and LOQC, respectively. The possibility to generate and manipulate subnatural-linewidth biphotons with low OD also opens up the opportunity to miniaturize the biphoton source for implementing quantum technologies on chip-scale quantum devices.

DOI: 10.1103/PhysRevA.101.063837

I. INTRODUCTION

Narrowband biphotons with subnatural linewidth play an indispensable role in photonic quantum technologies [1]. For example, the implementation of quantum repeaters [2] for long-distance quantum communication or large cluster states [3] for linear optical quantum computing relies on the photonic entanglement stored in quantum memories. The use of narrowband photons is thus advantageous for increasing the storage efficiency, particularly in the electromagnetically induced transparency-based (EIT-based) quantum memories [4–14]. Moreover, the possibility to manipulate the wave form of narrowband biphotons or heralded single photons has also made possible the faithful quantum-state mapping [15], high-efficiency quantum memory [16,17], efficient loading of single photons into a cavity [18], purification of a single photon [19], measurement of ultrashort biphotons [20], and revival of quantum interference and entanglement [21]. By manipulating the phase composition of the wave function, narrowband single photons can also be hidden in a noisy environment [22] and photon pairs can behave like fermions [23].

Narrowband biphotons or single photons can be realized by various mechanisms [24–41]. However, the efficient generation of subnatural-linewidth biphotons, which is advantageous for efficient light-matter interaction at the single-photon level, typically necessitates large (relative) group delays $\tau_g \approx L/V_g$ with high-optical-depth (high-OD) atomic ensembles, where L is the length of the atomic cloud and V_g is the anti-Stokes group velocity, or sophisticated optical cavities with parametric down-conversion. Here, by manipulating the two-component biphoton wave function in a low-OD atomic ensemble, we demonstrate subnatural-linewidth biphotons with a group delay that is tens of times smaller than previous works. Moreover, we achieve a biphoton linewidth in the sub-MHz regime with a limitation only imposed by the ground-state decoherence. Thanks to the possibility of controlling the quantum interference between the two-component biphotons, we also demonstrate the feasibility of shaping these biphotons and discuss their potential applications. As future quantum technologies require integrated optics architecture for improved performance and scalability, our work allows the miniaturization of a subnatural-linewidth biphoton or single-photon source for chip-scale quantum devices [42,43], where the realization of high OD is challenging.

This paper is organized as follows. In Sec. II, we discuss the key features of the biphoton generation exploiting off-resonance coupling field in spontaneous four-wave mixing (FWM). The experimental setup is then introduced in Sec. III. The demonstrations of the controlled quantum interference and sub-MHz-linewidth biphotons are described in Sec. IV and Sec. V, respectively. Finally, the applications of the spontaneous FWM with off-resonance coupling field are given in Sec. VI before we conclude our work in Sec. VII.

II. BIPHOTON GENERATION AT LOW OPTICAL DEPTH

Figure 1(a) illustrates the energy-level diagram used in our experiment, where the biphotons are generated through the spontaneous FWM [24–29]. In contrast to the previous works, where the EIT is exploited to obtain large group delays and narrow linewidths, the group delay in our experiment is kept small compared to other timescales in the system. Consequently, the EIT does not play a significant role; the large group delay and high OD are thus not necessary for obtaining the subnatural linewidth. Furthermore, as the large-group-delay scheme necessitates high ODs to achieve high efficiency for generating narrowband biphotons, our scheme can also realize a higher biphoton rate and brightness at moderate ODs. Nevertheless, the biphoton generation with

*ravi@phys.nthu.edu.tw
†cschuu@phys.nthu.edu.tw

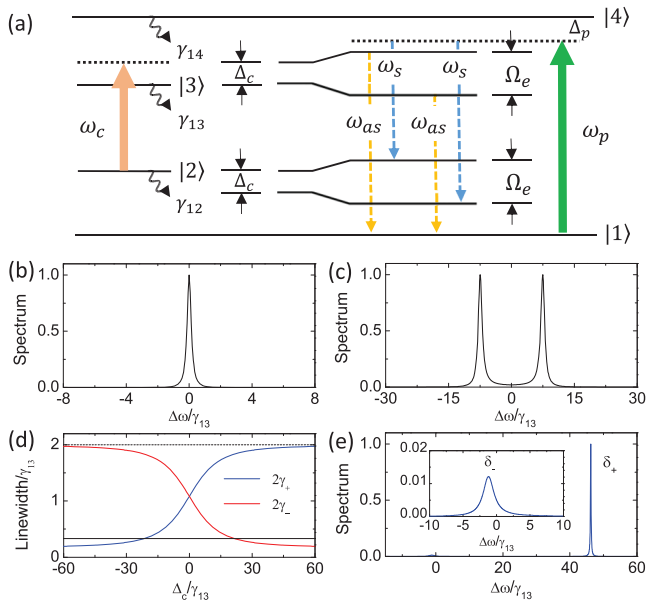

FIG. 1. (a) Energy-level diagram of the biphoton generation. If $\Delta_c = 0$, the biphotons either (b) are spectrally inseparable ($\Omega_c = 0.5\gamma_{13}$) or (c) have linewidths limited by $\gamma_{13} + \gamma_{12}$ ($\Omega_c = 15\gamma_{13}$). (d) If $\Delta_c \neq 0$, the biphoton linewidth is tunable by controlling Δ_c. The dashed and solid lines correspond to the natural linewidth and the MHz linewidth, respectively. (e) With $\Delta_c = 45\gamma_{13}$ ($\Omega_c = 14.8\gamma_{13}$), sub-MHz biphoton linewidth can be achieved with a dominant spectral power density.

small group delays typically results in either spectrally inseparable two-component biphotons or a linewidth limited by the dephasing rates of both the excited and ground states. To resolve these obstacles, we spectrally manipulate the two-component biphoton wave functions with an off-resonance coupling field, thus allowing us to demonstrate subnatural-linewidth biphotons in the sub-MHz regime with small group delay and low OD.

To elaborate the importance of the off-resonance coupling field, we consider the spontaneous FWM at low OD such that the group delay of the anti-Stokes photons is smaller than other timescales in the system. The wave function of the biphotons generated in this regime [44,45] (see the Appendix for more details), $\Psi(t_{as}, t_s) = \psi(\tau)\exp[-i(\omega_c + \omega_p)t_s]$, is predominantly determined by the third-order nonlinear susceptibility $\chi^{(3)}(\omega)$, where

$$\psi(\tau) \simeq -\frac{i\sqrt{\varpi_{as}\varpi_s}E_pE_cL}{\sqrt{8\pi}c}\int d\omega\chi^{(3)}(\omega)e^{-i\omega\tau}, \quad (1)$$

$\tau = t_{as} - t_s$ is the time delay between the detection of the anti-Stokes and Stokes photons, ϖ_{as} (ϖ_s) is the center frequency of the anti-Stokes (Stokes) photons, and E_p (E_c) is the amplitude of the pump (coupling) field. For $\Omega_c \gg |\gamma_{13} - \gamma_{12}|$,

$$\chi^{(3)}(\omega) \simeq \frac{-N\mu_{13}\mu_{32}\mu_{24}\mu_{41}/[4\varepsilon_0\hbar^3(\Delta_p + i\gamma_{14})]}{(\omega - \delta_+ + i\gamma_+)(\omega - \delta_- + i\gamma_-)}, \quad (2)$$

$$\delta_\pm = \tfrac{1}{2}(\Delta_c \pm \Omega_e), \quad (3)$$

$$\gamma_\pm = \frac{(\gamma_{13} + \gamma_{12})}{2} \pm \frac{\Delta_c}{\Omega_e}\frac{(\gamma_{13} - \gamma_{12})}{2}, \quad (4)$$

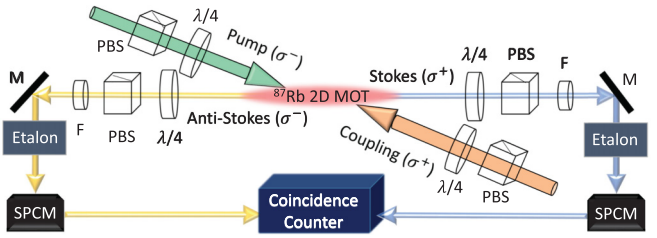

FIG. 2. Experimental setup. $\lambda/4$: quarter-wave plates; PBS: polarizing beam splitters; F: band-pass filters; M: mirrors; SPCM: single-photon counting modules.

where Δ_p (Δ_c) is the detuning of the pump (coupling) field, $\Omega_e = \sqrt{|\Omega_c|^2 + \Delta_c^2}$ is the effective Rabi frequency, γ_{1j} is the dephasing (spontaneous decay) rate of the state $|j\rangle$, N is the atomic density, and μ_{lm} is the atomic dipole moment of the $|l\rangle \leftrightarrow |m\rangle$ transition. The biphotons are thus composed of two frequency components resulting from two possible paths of FWM with red- and blue-detuned anti-Stokes photons (detuning of δ_- and δ_+), respectively. If the coupling field is on-resonance, the two-component biphotons either are spectrally inseparable [Fig. 1(b)] or have linewidths limited by $\gamma_{13} + \gamma_{12}$ [Fig. 1(c)].

If we introduce a detuning in the coupling field, the linewidths of these two components ($2\gamma_-$ and $2\gamma_+$) are both subnatural and can be tuned by controlling the coupling detuning Δ_c. This can be seen in Fig. 1(d), where we calculate the linewidths for $\gamma_{13} = 2\pi \times 3$ MHz, $\gamma_{12} = 0.084\gamma_{13}$, and $\Omega_c = 14.8\gamma_{13}$. For $\Delta_c > \Omega_c$ ($\Delta_c < -\Omega_c$), the linewidth $2\gamma_-$ ($2\gamma_+$) approaches $2\gamma_{12} = 0.17\gamma_{13}$ and is in the sub-MHz regime with a dominant spectral power density [Fig. 1(e)]. Compared to the large-group-delay scheme, the ultranarrow linewidth is thus achieved without the need of large group delay or high OD. In addition, the generation of the subnatural-linewidth biphotons is also more efficient at moderate ODs. For example, to achieve a biphoton linewidth of 0.3 MHz at $\gamma_{12} = 0.04\gamma_{13}$, the generation rate $R \sim |\Psi(t_{as}, t_s)|^2 t_c$ (t_c is the time bin) with OD = 5 will be 35 times higher than that of the large-group-delay scheme [45] with OD = 100. To put it another way, the large-group-delay scheme would need an OD higher than 3000, which is very challenging if not impossible with current technology, to obtain a similar rate.

III. EXPERIMENTAL SETUP

The schematic of our experimental setup is illustrated in Fig. 2. Time-energy-entangled photons are generated using an elongated cloud of ^{87}Rb atoms in a two-dimensional magneto-optical trap (2D MOT) with an OD of 5, where the relevant atomic levels are $|1\rangle = |5S_{1/2}, F = 1\rangle$, $|2\rangle = |5S_{1/2}, F = 2\rangle$, $|3\rangle = |5P_{1/2}, F = 2\rangle$, and $|4\rangle = |5P_{3/2}, F = 2\rangle$. More specifically, we drive the atomic ensemble with two counterpropagating fields at a tilt angle of 2.5°: the σ^+-polarized coupling field ω_c is detuned from $|2\rangle \leftrightarrow |3\rangle$ by Δ_c and the σ^--polarized pump field ω_p is red detuned from $|1\rangle \rightarrow |4\rangle$ by $14\gamma_{13}$. Through the FWM, phase-matched Stokes (ω_s, σ^+-polarized) and anti-Stokes (ω_{as}, σ^--polarized) photons are spontaneously generated in the backward-wave configuration. The generated Stokes and anti-Stokes photons

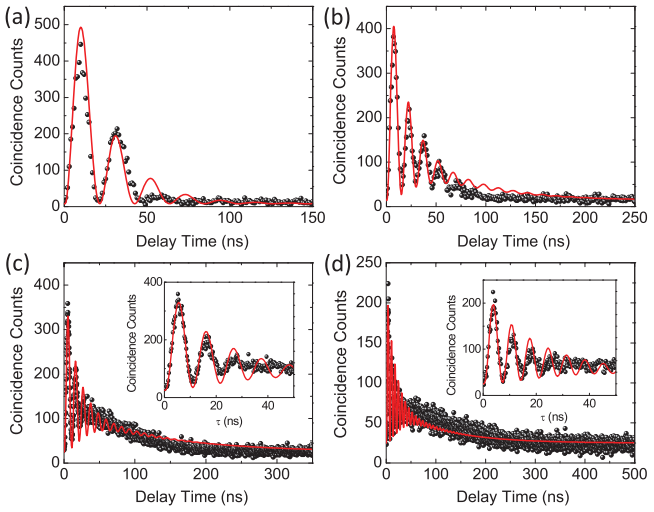

FIG. 3. Biphoton wave packets with (a) OD = 5, $\Delta_c = 0$, and $\Omega_c = 14.8\gamma_{13}$, (b) OD = 5, $\Delta_c = 16.7\gamma_{13}$, and $\Omega_c = 14.8\gamma_{13}$, (c) OD = 5, $\Delta_c = 28.3\gamma_{13}$, and $\Omega_c = 14.8\gamma_{13}$, and (d) OD = 5, $\Delta_c = 45\gamma_{13}$, and $\Omega_c = 14.8\gamma_{13}$. The measurement times are (a) 300, (b) 600, (c) 3600, and (d) 7200 s. The time bins are (a),(b) 1 and (c),(d) 0.25 ns.

pass through a set of polarization and band-pass filters and polarization-maintaining single-mode fibers with a coupling efficiency of 75%. Among these filters, we use a Fabry-Perot etalon with 15 MHz bandwidth in the anti-Stokes channel to spectrally select the subnatural-linewidth biphotons out of the two FWM channels. The temperature-stabilized etalon has a plano-convex geometry with a transmission and free spectral range of 12% and 22.9 GHz, respectively. The time-resolved coincidence counts of the biphotons are then registered by two single-photon counting modules (60% quantum efficiency) and a time-to-digital analyzer (0.25 or 1 ns time bin) for analyzing their temporal profiles.

IV. CONTROLLED QUANTUM INTERFERENCE

To generate the subnatural-linewidth biphotons at low OD, it is important to control the two-component biphoton wave function $\Psi(t_{as}, t_s)$ from the two possible FWM channels. Experimentally, this is observed by the Glauber correlation function (see the Appendix for more details),

$$G^{(2)}(\tau) = |\Psi(t_{as}, t_s)|^2 \propto [\, e^{-2\gamma_+\tau} + e^{-2\gamma_-\tau} - 2\cos(\Omega_e\tau)e^{-(\gamma_+ + \gamma_-)\tau}], \quad (5)$$

where the two components exhibit the exponential decays with widths inversely proportional to their linewidths. The quantum interference is revealed by their beating, of which the frequency and width are determined by Ω_e and $\gamma_+ + \gamma_-$, respectively. By changing the coupling detuning, we can thus control the ratio, linewidths, and beating of the two components. We demonstrate such ability by replacing the narrowband etalon (15 MHz bandwidth) in the anti-Stokes channel with a broadband etalon (500 MHz bandwidth) in order to observe their quantum interference. The measured biphoton wave packet for a resonant coupling field is shown in Fig. 3(a), which exhibits a beating pattern with a period equal to the frequency difference of the corresponding anti-Stokes photons, $\delta_+ - \delta_- = \Omega_c$. With $g_{s,as}(\tau)$ and $g_{s,s}(\tau)$ [or $g_{as,as}(\tau)$] denoting the normalized cross- and auto-correlation functions, respectively, we obtain $C(\tau) = g^2_{s,as}(\tau)/g_{s,s}(0)g_{as,as}(0) > 1$ with a peak value of $C_{\max} = 777 \pm 75$ at the maximum correlation, which violates the Cauchy-Schwarz inequality [46] and confirms the nonclassical correlation between the Stokes and anti-Stokes photons. The temporal correlation also exhibits a beating pattern with period equal to the frequency difference of the corresponding anti-Stokes photons, $\delta_+ - \delta_- = \Omega_c$, thus manifesting the presence of quantum interference between two possible paths of FWM. The biphoton wave packet can be described by the Glauber correlation function (see Appendix for more details),

$$G^{(2)}(\tau) \propto e^{-(\gamma_{13}+\gamma_{12})\tau}[1 - \cos(\Omega_c\tau)], \quad (6)$$

as given by the red curve in Fig. 3(a) with OD = 5, $\Omega_c = 14.8\gamma_{13}$, and $\gamma_{12} = 0.084\gamma_{13}$. As we increase the detuning of the coupling field Δ_c, the frequency difference $\delta_+ - \delta_- = \Omega_e$ between the two possible anti-Stokes or Stokes fields increases; the period of the beating thus decreases. This is evident in Figs. 3(b)–3(d) for the detunings of $16.7\gamma_{13}$, $28.3\gamma_{13}$, and $45\gamma_{13}$, respectively, where $C_{\max} = 126 \pm 13$, 48 ± 5, and 20 ± 3. The observed wave packets are in good agreement with the theory (red curves) for OD = 5, $\Omega_c = 14.8\gamma_{13}$, and $\gamma_{12} = 0.084\gamma_{13}$. Moreover, we observe the increase of the temporal length of biphoton wave packets to 95, 150, and 175 ns in Figs. 3(b)–3(d), respectively—an indication that the linewidth of the biphotons with blue-detuned anti-Stokes photons narrows as we increase the detuning [Eq. (4)]. In addition, the beating area also reduces as the detuning increases, which is consistent with the theory [Eqs. (2) to (4)] that a mismatch of linewidths or temporal lengths exists between the biphotons generated from two possible FWM.

V. SUBNATURAL-LINEWIDTH BIPHOTONS

The observed prolongation of the wave packet's temporal length verifies the feasibility to generate narrowband biphotons using low OD. For example, with coupling detunings of $16.7\gamma_{13}$, $28.3\gamma_{13}$, and $45\gamma_{13}$ in Figs. 3(b)–3(d), respectively, subnatural linewidths of $0.42\gamma_{13}$, $0.28\gamma_{13}$, and $0.22\gamma_{13}$ can be obtained if the biphotons with red-detuned anti-Stokes photons are discarded. To demonstrate this, we spectrally select the blue-detuned anti-Stokes photons using a Fabry-Perot etalon with 15 MHz bandwidth in the anti-Stokes channel. In addition, $\Omega_c = 16\gamma_{13}$ and $\Delta_c = 28.3\gamma_{13}$ are chosen so that the biphotons with blue- and red-detuned anti-Stokes photons have a frequency difference large enough to be distinguished by the narrowband etalon filter. Figure 4(a) shows the biphoton wave packet without the etalon filter at OD = 5. The quantum interference between the biphoton wave function from two possible FWMs is clearly observed with the beating frequency given by $\delta_+ - \delta_-$. With the insertion of the narrowband etalon filter transmitting only the blue-detuned anti-Stokes photons, the interference disappears, as shown in Fig. 4(b), where $C_{\max} = 5 \pm 1$. The resulting biphotons are now single frequency with a sub-MHz linewidth of $0.28\gamma_{13} \simeq$

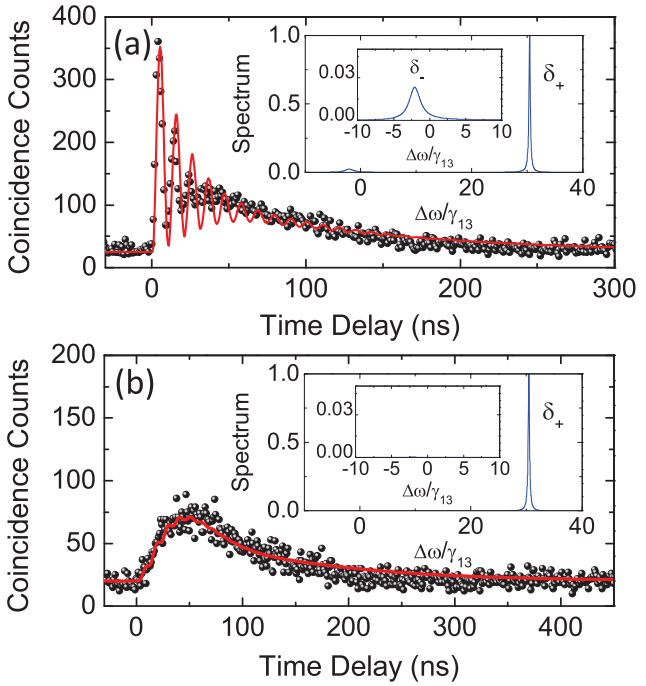

FIG. 4. Biphoton wave packets (a) without and (b) with the red-detuned anti-Stokes photons being discarded. The dots and curves are the experimental data (1 ns time bin and 7500 s measurement time) and theoretical fits, respectively. The corresponding spectra (arb. units) are shown in the insets.

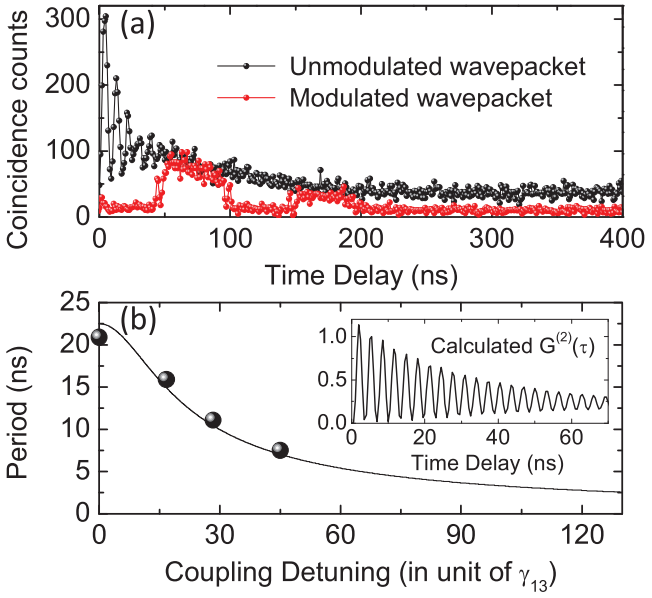

FIG. 5. (a) Unmodulated (black dots) and modulated (red dots) single-photon wave packets. (b) Measured periods of quantum interference as a function of the coupling detuning. The inset is the calculated wave packet with $\Delta_c = -100\gamma_{13}$ and $\Omega_c = 30\gamma_{13}$.

859 kHz and $\tau_g = 16$ ns as obtained by fitting the measured biphoton wave packet (black dots) with the theory (red curve), which takes into account the measured OD (5) and ground-state decay rate (252 kHz in the presence of magnetic field inhomogeneity from the magneto-optical trap). Correcting for the quantum efficiency of each detector (60%), the transmission of the broadband and narrowband etalon filters (45% and 2.6% including the fiber coupling) in the Stokes and anti-Stokes channels, respectively, the transmittance in each channel (50%), and duty cycle (20%), the generated paired rate is 10 368 s^{-1}. We note that the disappearance of the beating in Fig. 4(b) is also solid evidence of the quantum interference present with two possible FWMs, for example, in Figs. 3(a)–3(d) or Fig. 4(a).

VI. APPLICATIONS

The controlled quantum interference demonstrated here provides a useful means to shape the biphotons or heralded single photons generated by low-OD atomic ensembles, which were not previously preferred because of the short correlation time and the oscillatory pattern in their wave packets. As an example, in Fig. 5(a) (black dots), we utilize $\Delta_c = 28.3\gamma_{13}$ and $\Omega_c = 15\gamma_{13}$ without the narrowband etalon filter to prepare single (anti-Stokes) photons heralded by the detection of Stokes photons. The single-photon wave packet exhibits a long temporal length of 150 ns suitable for wave form or phase modulation [47]. More importantly, because of the temporal length mismatch between the wave functions of two possible FWMs, the oscillatory pattern is limited to the front of the wave packet and allows a large area behind for possible modulation. To modulate the wave packet, we pass the single photons through an electro-optic modulator (20 GHz bandwidth) driven by an arbitrary function generator (80 MHz modulation frequency). The modulator is triggered by the detection signal of the Stokes photons to ensure the synchronization of the arrivals of single photons and the modulation signal. For this purpose, a 35-m-long fiber is added in the beam path of anti-Stokes photons. The modulated single-photon wave packet with two 50-ns-long square pulses (separated by the pulse width) is shown by the red dots in Fig. 5(a); the modulation would not be possible with a resonant coupling field because the oscillatory pattern will occur all over the wave packet [Fig. 3(a)]. In addition to the arbitrary shaping of the wave packet, the quantum interference itself can also be utilized to realize single or entangled photons in a pulse train without the need for high-speed intensity modulators. Figure 5(b) shows the periods of quantum interference (dots) in Figs. 3(a)–3(d), which are in good agreement with the theory (curve) and tuned by controlling the coupling detuning. In the inset, we also show a calculated wave packet that exhibits a pulse train of 3 ns pulse width with $\Delta_c = -100\gamma_{13}$ and $\Omega_c = 30\gamma_{13}$.

VII. CONCLUSION

In summary, we have demonstrated biphotons with sub-natural linewidth in the sub-MHz regime utilizing an atomic ensemble with low OD. This is achieved by spectrally manipulating the two-component biphoton wave functions from two possible FWM channels. The biphoton linewidth is only limited by the ground-state decoherence in the presence of the magnetic field inhomogeneity from our magneto-optical trap. By switching off the magnetic field during the biphoton

generation, it is possible to reduce the ground-state decoherence further and obtain a narrower linewidth. The detuned biphotons are readily applicable to storage in the ultralow-noise room-temperature quantum memory [48] and can be frequency tuned to resonance by acousto-optic modulators (typical diffraction efficiency of 80%) if necessary. The temporally long biphotons, without the oscillatory pattern across the wave packet, also allows the arbitrary shaping of the photons and the generation of Bell states with subnatural linewidth [49] using a simpler setup.

ACKNOWLEDGMENTS

The authors thank P. K. Chen, C. W. Yang, W. L. Hung, and C. H. Kuo for their experimental assistance or helpful discussion. This work was supported by the Ministry of Science and Technology, Taiwan (Grants No. 107-2112-M-007-004-MY3 and No. 107-2745-M-007-001).

APPENDIX: BIPHOTON WAVE PACKET

In the perturbation theory [44,45], the biphoton state is given by

$$|\Psi\rangle = -\frac{i}{\hbar}\int_{-\infty}^{+\infty} dt \hat{H}_I|0\rangle, \tag{A1}$$

where the interaction Hamiltonian is

$$H_I = \frac{\varepsilon_0 A}{2}\int_{-L/2}^{L/2} dz \chi^{(3)} E_p^{(+)} E_c^{(+)} \hat{E}_s^{(-)} \hat{E}_{as}^{(-)} + \text{H.c.}, \tag{A2}$$

A is the single-mode cross-section area, in which the generated fields are collected for the correlation measurement, and L is the length of the atomic ensemble. The positive-frequency part of the pump and coupling fields are described by

$$\begin{aligned} E_p^{(+)}(z,t) &= E_p e^{i(k_p z-\omega_p t)}, \\ E_c^{(+)}(z,t) &= E_c e^{i(-k_c z-\omega_c t)}, \end{aligned} \tag{A3}$$

where E_p and E_c are the corresponding electric-field amplitudes. $\hat{E}_s^{(-)}$ and $\hat{E}_{as}^{(-)}$ are the single-transverse-mode operators of the Stokes and anti-Stokes fields,

$$\begin{aligned} \hat{E}_s^{(-)}(z,t) &= \sqrt{\frac{\hbar\varpi_s}{c\varepsilon_0\pi A}}\int d\omega \hat{a}_s^\dagger(\omega) e^{i(k_s(\omega)z-\omega t)}, \\ \hat{E}_{as}^{(-)}(z,t) &= \sqrt{\frac{\hbar\varpi_{as}}{c\varepsilon_0\pi A}}\int d\omega \hat{a}_{as}^\dagger(\omega) e^{i(-k_{as}(\omega)z-\omega t)}. \end{aligned} \tag{A4}$$

Here, $\hat{a}_s^\dagger(\omega)$ and $\hat{a}_{as}^\dagger(\omega)$ are the creation operators of the Stokes and anti-Stokes fields, respectively, which obey the commutation relations $[\hat{a}_s(\omega), \hat{a}_s^\dagger(\omega')]=[\hat{a}_{as}(\omega), \hat{a}_{as}^\dagger(\omega')]=\delta(\omega-\omega')$, and ϖ_s (ϖ_{as}) is the center frequency of the Stokes (anti-Stokes) field.

Using Eq. (A3) and Eq. (A4), the interaction Hamiltonian and biphoton state can be obtained as follows:

$$\begin{aligned} \hat{H}_I = \frac{i\hbar L}{2\pi}\int d\omega_{as} d\omega_s \kappa(\omega_{as},\omega_s)\text{sinc}\left(\frac{\Delta kL}{2}\right) \\ \times \hat{a}_{as}^\dagger(\omega_{as})\hat{a}_s^\dagger(\omega_s) e^{-i(\omega_c+\omega_p-\omega_{as}-\omega_s)t} + \text{H.c.}, \end{aligned} \tag{A5}$$

$$\begin{aligned} |\Psi\rangle = L\int d\omega_{as}\kappa(\omega_{as},\omega_p+\omega_c-\omega_{as})\text{sinc}\left(\frac{\Delta kL}{2}\right) \\ \times \hat{a}_{as}^\dagger(\omega_{as})\hat{a}_s^\dagger(\omega_p+\omega_c-\omega_{as})|0\rangle, \end{aligned} \tag{A6}$$

where $\Delta k = k_{as}-k_s-(k_c-k_p)$ is the phase-mismatch function, $\kappa(\omega_{as},\omega_s) = -i(\sqrt{\varpi_{as}\varpi_s}/2c)\chi^{(3)}(\omega_{as})E_pE_c$ is the nonlinear parametric coupling coefficient, and

$$\chi^{(3)}(\omega) = \frac{N\mu_{13}\mu_{32}\mu_{24}\mu_{41}}{\varepsilon_0\hbar^3(\Delta_p+i\gamma_{14})D(\omega)} \tag{A7}$$

is the third-order nonlinear susceptibility [50–52] with $D(\omega) = |\Omega_c|^2 - 4(\omega+i\gamma_{13})(\omega-\Delta_c+i\gamma_{12})$. Here, N is the atomic density, Δ_p and Δ_c are the detunings of the pump and coupling fields, respectively, γ_{1j} is the dephasing (spontaneous decay) rate of the state $|j\rangle$, $\Omega_c = \mu_{23}E_c/\hbar$ is the Rabi frequency of the coupling field with E_c being the complex amplitude of the electric field, and μ_{lm} is the atomic dipole moment associated with the transition $|l\rangle \leftrightarrow |m\rangle$.

The Glauber correlation function is defined by

$$\begin{aligned} G^{(2)}(t_{as},t_s) &= \langle\Psi|\hat{a}_s^\dagger(t_s)\hat{a}_{as}^\dagger(t_{as})\hat{a}_{as}(t_{as})\hat{a}_s(t_s)|\Psi\rangle \\ &= |\Psi(t_{as},t_s)|^2. \end{aligned} \tag{A8}$$

Here, $\hat{a}_s(t_s)$ and $\hat{a}_{as}(t_{as})$ are the annihilation operators of the Stokes and anti-Stokes fields, respectively, in the time domain. $\Psi(t_{as},t_s)$ is the biphoton wave function,

$$\Psi(t_{as},t_s) = \psi(\tau)e^{-i(\omega_c+\omega_p)t_s}, \tag{A9}$$

where

$$\psi(\tau) = \frac{L}{2\pi}\int d\omega_{as}\kappa(\omega_{as})\Phi(\omega_{as})e^{-i\omega_{as}\tau}, \tag{A10}$$

$\tau = t_{as}-t_s$ is the time delay between the detection of the anti-Stokes and Stokes photons, and $\Phi(\omega_{as})$ is the longitudinal detuning function,

$$\Phi(\omega_{as}) = \text{sinc}\left(\frac{\Delta kL}{2}\right)e^{i(k_{as}+k_s)L/2}. \tag{A11}$$

In this work, the biphoton wave function is dominated by $\kappa(\omega)$, which is associated with the third-order nonlinear susceptibility $\chi^{(3)}$, so that

$$\psi(\tau) \simeq -\frac{i\sqrt{\varpi_s\varpi_{as}}E_pE_cL}{\sqrt{8\pi}c}\int d\omega \chi^3(\omega)e^{-i\omega\tau}. \tag{A12}$$

By substituting Eq. (A7) into the above equation,

$$\psi(\tau) \simeq C\int d\omega \frac{e^{-i\omega\tau}}{(\omega-\delta_+ +i\gamma_+)(\omega-\delta_- +i\gamma_-)}, \tag{A13}$$

where $C = -i\sqrt{\varpi_s\varpi_{as}}E_pE_cLN\mu_{13}\mu_{32}\mu_{24}\mu_{41}e^{-i\varpi_{as}\tau}/\sqrt{8\pi}c\varepsilon_0\hbar^3(\Delta_p+i\gamma_{14})$. The Glauber correlation function

can then be evaluated using the residue theorem to be

$$G^{(2)}(\tau) = \tfrac{1}{2}|C|^2[e^{-2\gamma_+\tau} + e^{-2\gamma_-\tau} - 2\cos(\Omega_e\tau)e^{-(\gamma_+ + \gamma_-)\tau}]\Theta(\tau), \quad \text{(A14)}$$

where $\Theta(\tau)$ is the Heaviside step function. If the coupling is on-resonance, $\Delta_c = 0$, it can be reduced to

$$G^{(2)}(\tau) = \tfrac{1}{2}|C|^2 e^{-2(\gamma_{13}+\gamma_{12})\tau}[1 - \cos(\Omega_c\tau)]\Theta(\tau). \quad \text{(A15)}$$

[1] *Engineering the Atom-photon Interaction*, edited by A. Predojević and M. W. Mitchell (Springer International Publishing, Switzerland, 2015).

[2] H.-J. Briegel, W. Dür, J. I. Cirac, and P. Zoller, Phys. Rev. Lett. **81**, 5932 (1998).

[3] D. E. Browne and T. Rudolph, Phys. Rev. Lett. **95**, 010501 (2005).

[4] C. Liu, Z. Dutton, C. H. Behroozi, and L. V. Hau, Nature (London) **409**, 490 (2001).

[5] D. F. Phillips, A. Fleischhauer, A. Mair, R. L. Walsworth, and M. D. Lukin, Phys. Rev. Lett. **86**, 783 (2001).

[6] A. Kuzmich, W. P. Bowen, A. D. Boozer, A. Boca, C. W. Chou, L.-M. Duan, and H. J. Kimble, Nature (London) **423**, 731 (2003).

[7] D. N. Matsukevich, T. Chanelière, S. D. Jenkins, S.-Y. Lan, T. A. B. Kennedy, and A. Kuzmich, Phys. Rev. Lett. **97**, 013601 (2006).

[8] S. Chen, Y.-A. Chen, T. Strassel, Z.-S. Yuan, B. Zhao, J. Schmiedmayer, and J.-W. Pan, Phys. Rev. Lett. **97**, 173004 (2006).

[9] C.-S. Chuu, T. Strassel, B. Zhao, M. Koch, Y.-A. Chen, S. Chen, Z.-S. Yuan, J. Schmiedmayer, and J.-W. Pan, Phys. Rev. Lett. **101**, 120501 (2008).

[10] R. Zhao, Y. O. Dudin, S. D. Jenkins, C. J. Campbell, D. N. Matsukevich, T. A. B. Kennedy, and A. Kuzmich, Nat. Phys. **5**, 100 (2009).

[11] B. Zhao, Y.-A. Chen, X.-H. Bao, T. Strassel, C.-S. Chuu, X.-M. Jin, J. Schmiedmayer, Z.-S. Yuan, S. Chen, and J.-W. Pan, Nat. Phys. **5**, 95 (2009).

[12] Y.-H. Chen, M.-J. Lee, I.-Chung Wang, S. Du, Y.-F. Chen, Y.-C. Chen, and I. A. Yu, Phys. Rev. Lett. **110**, 083601 (2013).

[13] Y.-F. Hsiao, P.-J. Tsai, H.-S. Chen, S.-X. Lin, C.-C. Hung, C.-H. Lee, Y.-H. Chen, Y.-F. Chen, I. A. Yu, and Y.-C. Chen, Phys. Rev. Lett. **120**, 183602 (2018).

[14] Y. Wang, J. Li, S. Zhang, K. Su, Y. Zhou, K. Liao, S. Du, H. Yan, and S.-L. Zhu, Nat. Photon. **13**, 346 (2019).

[15] J. I. Cirac, P. Zoller, H. J. Kimble, and H. Mabuchi, Phys. Rev. Lett. **78**, 3221 (1997).

[16] A. V. Gorshkov, A. André, M. Fleischhauer, A. S. Sørensen, and M. D. Lukin, Phys. Rev. Lett. **98**, 123601 (2007).

[17] S. Zhang, C. Liu, S. Zhou, C.-S. Chuu, M. M. T. Loy, and S. Du, Phys. Rev. Lett. **109**, 263601 (2012).

[18] C. Liu, Y. Sun, L. Zhao, S. Zhang, M. M. T. Loy, and S. Du, Phys. Rev. Lett. **113**, 133601 (2014).

[19] S.-W. Feng, C.-Y. Cheng, C.-Y. Wei, J.-H. Yang, Y.-R. Chen, Y.-W. Chuang, Y.-H. Fan, and C.-S. Chuu, Phys. Rev. Lett. **119**, 143601 (2017).

[20] C. Belthangady, S. Du, C.-S. Chuu, G.-Y. Yin, and S. E. Harris, Phys. Rev. A **80**, 031803(R) (2009).

[21] C.-H. Wu, C.-K. Liu, Y.-C. Chen, and C.-S. Chuu, Phys. Rev. Lett. **123**, 143601 (2019).

[22] C. Belthangady, C.-S. Chuu, I. A. Yu, G. Y. Yin, J. M. Kahn, and S. E. Harris, Phys. Rev. Lett. **104**, 223601 (2010).

[23] H. P. Specht, J. Bochmann, M. Mücke, B. Weber, E. Figueroa, D. L. Moehring, and G. Rempe, Nat. Photon. **3**, 469 (2009).

[24] V. Balić, D. A. Braje, P. Kolchin, G. Y. Yin, and S. E. Harris, Phys. Rev. Lett. **94**, 183601 (2005).

[25] S. Du, P. Kolchin, C. Belthangady, G. Y. Yin, and S. E. Harris, Phys. Rev. Lett. **100**, 183603 (2008).

[26] B. Srivathsan, G. K. Gulati, B. Chng, G. Maslennikov, D. Matsukevich, and C. Kurtsiefer, Phys. Rev. Lett. **111**, 123602 (2013).

[27] L. Zhao, X. Guo, C. Liu, Y. Sun, M. M. T. Loy, and S. Du, Optica **1**, 84 (2014).

[28] C. Shu, P. Chen, T. K. A. Chow, L. Zhu, Y. Xiao, M. M. T. Loy, and S. Du, Nat. Commun. **7**, 12783 (2016).

[29] X. Guo, Y. Mei, and S. Du, Optica **4**, 388 (2017).

[30] C. E. Kuklewicz, F. N. C. Wong, and J. H. Shapiro, Phys. Rev. Lett. **97**, 223601 (2006).

[31] X.-H. Bao, Y. Qian, J. Yang, H. Zhang, Z.-B. Chen, T. Yang, and J.-W. Pan, Phys. Rev. Lett. **101**, 190501 (2008).

[32] M. Scholz, L. Koch, and O. Benson, Phys. Rev. Lett. **102**, 063603 (2009).

[33] F. Wolfgramm, Y. A. de Icaza Astiz, F. A. Beduini, A. Cerè, and M. W. Mitchell, Phys. Rev. Lett. **106**, 053602 (2011).

[34] M. Rambacha, A. Nikolova, T. J. Weinhold, and A. G. White, APL Photon. **1**, 096101 (2016).

[35] C.-H. Wu, T.-Y. Wu, Y.-C. Yeh, P.-H. Liu, C.-H. Chang, C.-K. Liu, T. Cheng, and C.-S. Chuu, Phys. Rev. A **96**, 023811 (2017).

[36] A. Kuhn, M. Hennrich, and G. Rempe, Phys. Rev. Lett. **89**, 067901 (2002).

[37] H. P. Keller, B. Lange, K. Hayasaka, W. Lange, and H. Walther, Nature (London) **431**, 1075 (2004).

[38] J. McKeever, A. Boca, A. D. Boozer, R. Miller, J. R. Buck, A. Kuzmich, and H. J. Kimble, Science **303**, 1992 (2004).

[39] J. K. Thompson, J. Simon, H. Loh, and V. Vuletić, Science **313**, 74 (2006).

[40] L.-M. Duan, M. D. Lukin, J. I. Cirac, and P. Zoller, Nature (London) **414**, 413 (2001).

[41] P. Farrera, G. Heinze, B. Albrecht, M. Ho, M. Chávez, C. Teo, N. Sangouard, and H. de Riedmatten, Nat. Commun. **7**, 13556 (2016).

[42] J. Fortágh and C. Zimmermann, Rev. Mod. Phys. **79**, 235 (2007).

[43] *Atom Chips*, edited by J. Reichel and V. Vuletic (Wiley-VCH, Germany, 2011).

[44] J. Wen, S. Du, and M. H. Rubin, Phys. Rev. A **76**, 013825 (2007).

[45] S. Du, J. Wen, and M. H. Rubin, J. Opt. Soc. Am. B **25**, C98 (2008).
[46] J. F. Clauser, Phys. Rev. D **9**, 853 (1974).
[47] P. Kolchin, C. Belthangady, S. Du, G. Y. Yin, and S. E. Harris, Phys. Rev. Lett. **101**, 103601 (2008).
[48] M. Namazi, C. Kupchak, B. Jordaan, R. Shahrokhshahi, and E. Figueroa, Phys. Rev. Appl. **8**, 034023 (2017).
[49] K. Liao, H. Yan, J. He, S. Du, Z.-M. Zhang, and S.-L. Zhu, Phys. Rev. Lett. **112**, 243602 (2014).
[50] D. A. Braje, V. Balić, S. Goda, G. Y. Yin, and S. E. Harris, Phys. Rev. Lett. **93**, 183601 (2004).
[51] J.-M. Wen and M. H. Rubin, Phys. Rev. A **74**, 023808 (2006).
[52] J.-M. Wen and M. H. Rubin, Phys. Rev. A **74**, 023809 (2006).